Electron. Mater. Lett., Vol. 10, No. 1 (2014), pp. 81-87
DOI: 10.1007/s13391-013-3130-2

Hydrothermally Grown Boron-Doped ZnO Nanorods for Various Applications: Structural, Optical, and Electrical Properties

Soaram Kim,[1] Hyunggil Park,[1] Giwoong Nam,[1] Hyunsik Yoon,[1] Byunggu Kim,[2] Iksoo Ji,[2] Younggyu Kim,[2] Ikhyun Kim,[2] Youngbin Park,[2] Daeho Kang,[2] and Jae-Young Leem[1,2,*]

[1]Department of Nano Systems Engineering, Center for Nano Manufacturing, Inje University, Gimhae, Gyungnam 621-749, Korea
[2]Department of Nano Engineering, Inje University, Gimhae, Gyungnam 621-749, Korea

(received date: 8 May 2013 / accepted date: 3 June 2013 / published date: 10 January 2014)

The structural, optical, and electrical properties of ZnO and BZO nanorods were investigated using field-emission scanning electron microscopy, x-ray diffraction (XRD), photoluminescence (PL), and van der Pauw Hall-effect measurements. All the nanorods had grown well on the ZnO seed layers and were hexagonal. The BZO nanorods were shorter than the undoped ZnO nanorods, and the BZO nanorods grew shorter with increasing concentration of B to 2.0 at. % while the average length of the nanorods doped with 2.5 at. % B increased from 1620 to 1830 nm. The XRD patterns suggest that the amount of residual stress in the nanorods decreased with increasing concentration of B in the nanorods. The PL spectra showed near-band-edge and deep-level emissions, and B doping also varied the PL properties of the ZnO nanorods. The Hall-effect data suggest that B doping also varied the electrical properties such as the carrier concentration, mobility, and resistivity of the ZnO nanorods.

Keywords: zinc oxide, B-doped, hydrothermal, nanorods, photoluminescence, hall-effect

1. INTRODUCTION

Zinc oxide (ZnO) is one of the most important semiconductor materials because of its wide bandgap (3.37 eV) and useful electro-optic and electro-mechanical properties, including piezoelectricity, UV luminescence, high exciton binding energy (60 meV), high electron mobility, and chemical/thermal stability.[1-5] In recent years, there have been numerous studies on the synthesis and applications of ZnO nanostructures such as one-dimensional ZnO nanorods in dye-sensitized solar cells and thermoelectronics.[6-8] ZnO nanorods have conventionally been grown using numerous methods, such as chemical vapor deposition (CVD),[9] vapor phase transport (VPT),[10] and hydrothermal synthesis.[11] In gerneral, CVD and VPT usually require high operation temperature and complicated systems for growth. However, hydrothermal synthesis enables the preparation of ZnO nanorods at much lower temperatures than CVD and VPT do, which makes the process more effective, simplifies the control of dopant concentrations, and enables the use of simple equipment.[12] Hydrothermal synthesis of ZnO nanorods can be summarized in three steps as follows: ZnO seed layers are first deposited onto a suitable substrate such as quartz. This is perhaps the most important step of the three because the seed layers serve as the foundation upon which the nanorods will grow; hence, the quality of the seed layers is the factor that most significantly affects the quality of the final nanorods. Randomly oriented ZnO crystals are then grown from the seed layers. Finally, extended ZnO nanorods are grown through collisions among the randomly oriented ZnO crystals, to form arrays of nanorods whose *c*-axis are oriented perpendicular to the substrate surface.[13]

In general, group III elements such as B,[14,15] Al,[16,17] Ga,[18,19] and In[20,21] can be used as cation dopants to improve the optical and electrical properties of ZnO nanorods. Al-Ga-, In-, and B-doped ZnO (BZO), nanorods can be used as transparent electrodes in optoelectronic devices. Consequently, considerable efforts have been devoted toward doping ZnO nanorods to improve their optical and electrical properties. Furthermore, doping can also be used to effectively tune the band gap of ZnO, which will in turn affect the optical properties of ZnO.[22-24] Among the various kinds of doped ZnO, the BZO has recently been extensively investigated because of its ferromagnetic properties[25] and for its utilitarian application in dye-sensitized solar cells[26] and as a TCO material.[27] B doping can improve the density and mobility of carriers in and the electrical conductivity of ZnO,[27] and it increases the magnetic moment of ZnO,[25] which is quite different from where the magnetic properties

*Corresponding author: jyleem@inje.ac.kr

of ZnO[28,29] doped with other elements originate. Moreover, B doping also results in higher quantum efficiency at near-infrared region, and thus renders BZO material suitable for application to the transparent window layers of copper indium gallium selenide (CIGS) solar cells.[30]

Although there are numerous reports on ZnO nanorods systematically doped with various dopants, there are few published reports to date on the properties of hydrothermally grown BZO nanorods as far as we know. Yu *et al.*[14,31] reported improved properties of the BZO nanorods grown on opaque substrates (*i.e.*, silicon substrates) using hydrothermal synthesis. However, it is needed that the ability to grow the BZO nanorods onto transparent substrates for a future generation of smart and functional applications. Hence, in this study, we investigated how B doping affects the structural, optical, and electrical properties of ZnO nanorods on transparent substrates (*i.e.*, quartz substrates) for various applications.

2. EXPERIMENTAL PROCEDURE

Sol-gel spin-coating was used to deposit ZnO seed layers onto quartz substrates. The sol solution was prepared by dissolving 0.6 M zinc acetate dihydrate [$Zn(CH_3OO)_2{\cdot}2H_2O$] in 0.6 M 2-methoxyethanol and monoethanolamine (MEA) was then added to stabilize the sol solution. The molar ratio of zinc acetate to MEA was 1 : 1 for all trials. The stabilized sol solution was stirred at 60°C for 2 h to produce a clear, homogeneous solution that was subsequently aged at room temperature for 24 h. The aged sol solution was spin-coated onto the quartz substrates rotating at 3,000 rpm for 20 s to produce ZnO seed layers, which were subsequently pre-heated at 300°C for 10 min to evaporate the solvent and remove any residual organic materials. The preheated ZnO seed layers were cooled at 5°C/min to prevent the formation of cracks. The ZnO seed layers were coated, pre-heated, and cooled three times each and were then post-heated in air in furnace at 550°C for 1 h.

The ZnO and BZO nanorods were then hydrothermally grown on the postheated ZnO seed layers. Five aqueous solutions, one of which was only pure deionized (DI) water and the other four of which contained the salt triisopropyl borate [$((CH_3)_2CHO)_3B$], whose B concentrations were 0 (*i.e.*, undoped ZnO), 0.5, 1.0, 2.0, or 2.5 at. % were used as B^{3+} cation dopant precursors. Each ZnO seed layer was first rinsed with DI water and was then immersed in a mixture of aqueous 0.1 M zinc nitrate hexahydrate [$Zn(NO_3)_2{\cdot}6H_2O$], 0.1 M hexamethylenetetramine (HMT) [$(CH_2)_6N_4$], and one of the five an aqueous solutions containing the B^{3+} cation dopant precursor. The mixtures containing the seed layers were then confined in a Teflon-lined autoclave. The nanorods were hydrothermally grown by maintaining the autoclave at 95°C for 4 h. After the reaction had completed, the hydrothermally grown nanorods were rinsed with DI water and blow-dried with ultra-high-purity (*i.e.*, 99.9999%) nitrogen to remove any unreacted residual salts and organic materials. The structural, optical, and electrical properties of the hydrothermally grown ZnO nanorods doped with 0 - 2.5 at. % B were investigated using scanning electron microscopy (SEM), x-ray diffraction (XRD), photoluminescence (PL), and van der Pauw Hall-effect measurements.

3. RESULTS AND DISCUSSION

Figure 1 shows the SEM images of the ZnO nanorods doped with (a) 0 (*i.e.*, undoped ZnO), (b) 0.5, (c) 1.0, (d) 2.0, and (e) 2.5 at. % B, and the nanorods were on average 2650, 2025, 1995, 1620, and 1830 nm long, respectively. All the nanorods had grown well on the ZnO seed layers and were hexagonal. Interestingly, all the BZO nanorods were shorter than the undoped ZnO nanorods, and the BZO nanorods grew shorter with increasing concentration of B to 2.0 at. %. This is because B^{3+} ions are trivalent; hence, the concentration of Zn^{2+} intersititial ions was decreased to compensate for the difference in the charge of the B-doped crystal lattice, suppressing the growth of the ZnO nanorods.[32,33] However, the average length of the nanorods doped with 2.5 at. % B increased from 1620 to 1830 nm, which may indicate that the ZnO lattice had been doped with interstitial B^{3+} ions and/or that Zn^{2+} ions in the lattice had been substituted with the higher valence B^{3+} ions, which in turn lengthened the nanorods.[16] It is notable that we could control the length of the nanorods by adding B while the nanorods were growing.

Figure 2(a) shows the XRD patterns for the ZnO nanorods doped with 0 - 2.5 at. % B. The patterns for all the BZO nanorods are dominated by the (002) peak associated with wurtzite ZnO, implying that the preferred growth orientation of the BZO nanorods is along the (002) direction because their vertical growth was rapid and their lateral growth was relatively limited.[34] Furthermore, certain additives may modify the energy of the (002) surface; hence, significantly affecting the rate at which ZnO nanorods grow along the (002) direction. The intensity of the (002) peak decreased with increasing concentration of B in the nanorods, as shown Fig. 2(b), because the intensity of the (002) peak is proportional to the length and density of the nanorods. In addition, the position of the (002) peak shifted to a lower angle with increasing concentration of B in the nanorods, indicating that the ZnO lattice had been doped with B. The radius of the B^{3+} ions is smaller than that of the Zn^{2+} ion. Therefore, the interstitial Zn^{2+} ions with B^{3+} ions will shift the position of the (002) peak to a lower angle. The difference between the ionic radii of Zn^{2+} and B^{3+} is likely responsible for the distortion of the ZnO lattice. The lattice constants for as-grown ZnO ($a = 0.32498$ nm and $c = 0.52066$ nm) are generally close to those that by Heller *et al*. reported.[35] In

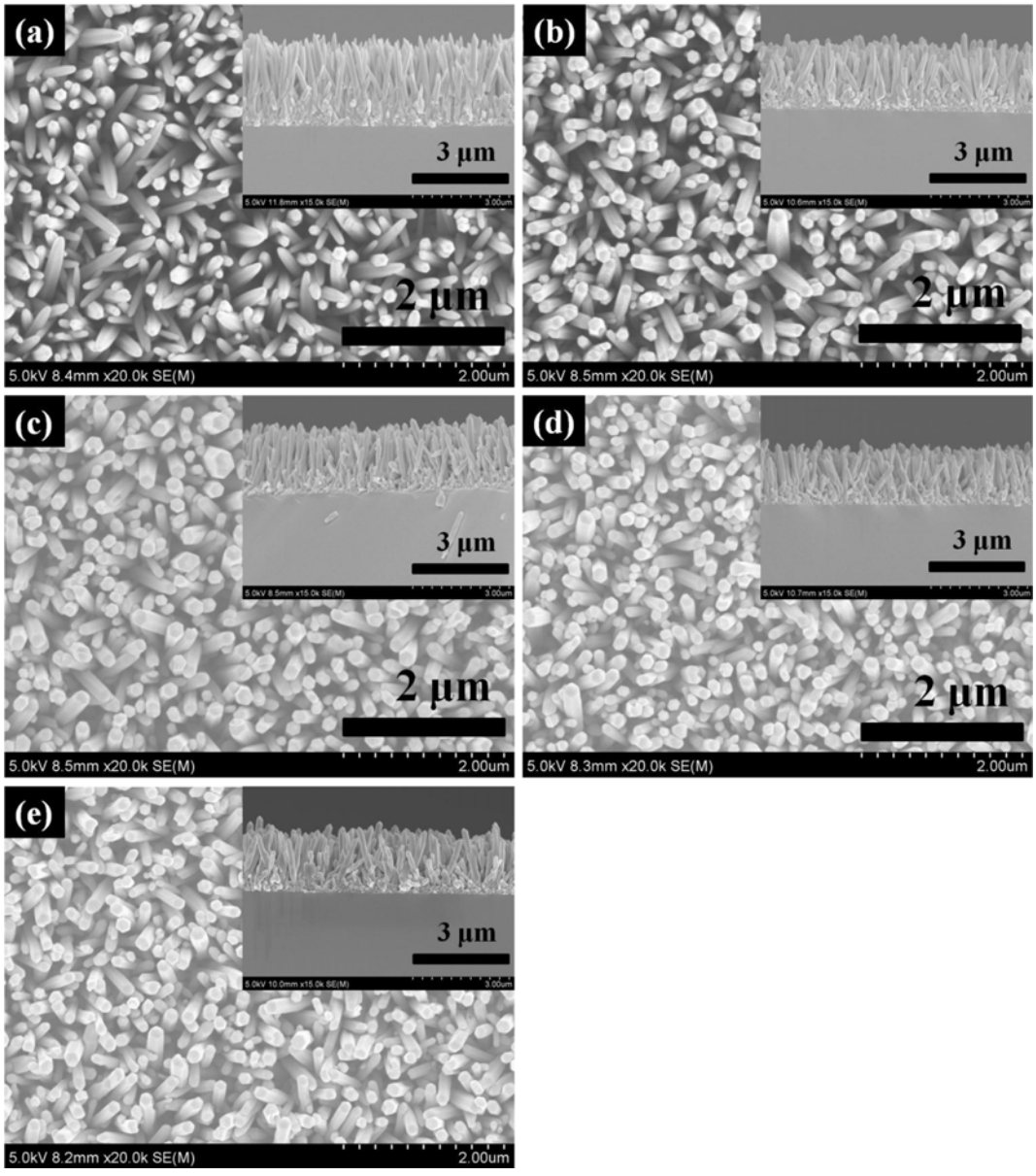

Fig. 1. SEM images of ZnO nanorods doped with (a) 0 (*i.e.*, undoped ZnO nanorods), (b) 0.5, (c) 1.0, (d) 2.0, and (e) 2.5 at. % B.

our experiments, the lattice constants for ZnO varied from $a = 0.32277$ and $c = 0.51751$ nm for the undoped ZnO nanorods to $a = 0.32313$ and $c = 0.51808$ nm for the ZnO nanorods doped with 2.5 at. % B, as shown in Fig. 2(c). The lattice constants for ZnO can be calculated as follows:[36]

$$c = 2d_{002} = \lambda/\sin\theta \quad (1)$$

where λ represents the wavelength of the Cu-$K\alpha$ radiation (1.5406 Å) and θ represents the Bragg angle. The difference in the ZnO lattice constants is significant, which suggests that the B atoms occupied specific sites in the ZnO lattice, resulting in anisotropic distortion along the (001) direction of the unit cell of the ZnO crystal. Therefore, doping the ZnO lattice with B considerably distorts the ZnO lattice and accordingly affects the lattice structure and/or crystallinity of the ZnO nanorods. Interestingly, the B-doping-induced change in the lattice structure and/or crystallinity of the ZnO nanorods is desirable because the ZnO lattice constants for the ZnO nanorods doped with 2.5 at. % B are close to the reported values, which may indicate that B doping decreased the number of opint defects in the ZnO lattice. The increase in the ZnO lattice constants and the shift in the position of the (002) peaks to a lower angle with increasing concentration of B in the nanorods implies that the amount of residual stress in the BZO nanorods was higher than that in strain-free ZnO and that the amount of residual stress in the BZO

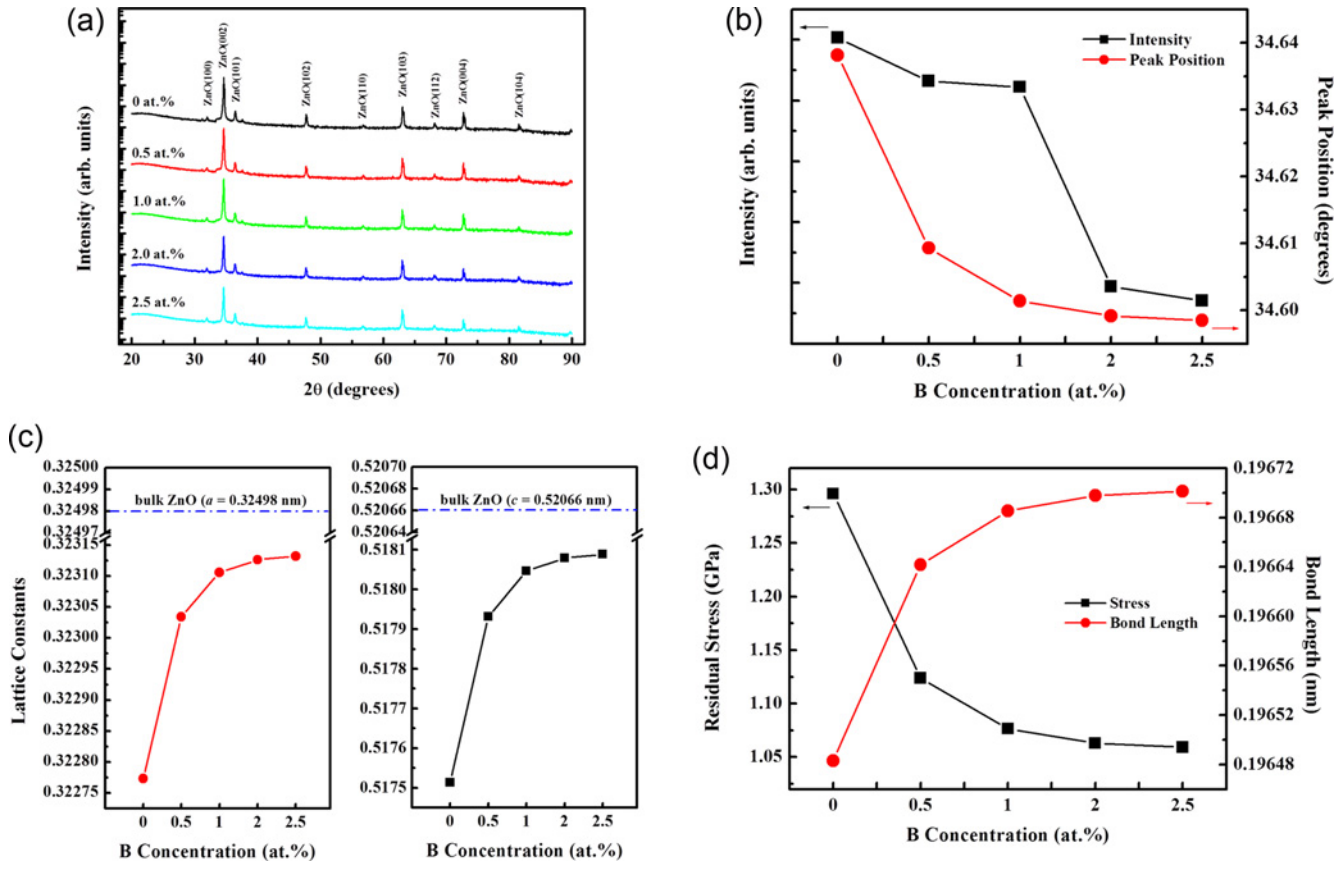

Fig. 2. (a) XRD patterns, (b) intensity and position of peaks, (c) lattice constants, and (d) residual stress and bond length of crystal lattice in ZnO nanorods doped with 0 - 2.5 at. % B.

nanorods decreased with increasing concentration of B in the nanorods. The magnitude of the residual stress (σ) and the length of the bonds in the ZnO crystal lattice (*i.e.*, bond length (L)) are plotted as functions of the concentration of B in the nanorods (Fig. 2(d)) to better understand the effect of B doping on the amount of residual stress in the ZnO nanorods. Residual stress is generated in the ZnO nanorods because of the differences between the lattice constants and thermal expansion coefficients of the ZnO and the quartz substrate. The amount of residual stress in the ZnO nanorods can be calculated as follows:[37]

$$\sigma = [2C_{13}^2 - C_{33}(C_{11}+C_{12})/2C_{13}] \times [(c-c_0)/c_0] \quad (2)$$

where C_{ij} represent the elastic stiffness constants for ZnO (*i.e.*, $C_{11} = 207.0$, $C_{33} = 209.5$, $C_{12} = 117.7$, and $C_{13} = 106.1$ GPa), and c and c_0 are the lattice parameters for the ZnO and strain-free ZnO, respectively. The biaxial stress will be tensile if the sign of the stress is positive and compressive if the sign of the stress is negative. The amounts of residual stress in the ZnO nanorods doped with 0, 0.5, 1.0, 2.0, and 2.5 at. % B were 1.29598, 1.12372, 1.07644, 1.06299, and 1.05910 GPa, respectively. Therefore, the amount of residual stress in the ZnO nanorods doped with 2.5 at. % B is close to that in strain-free ZnO. The average length of the Zn-O in the ZnO crystal lattice is given by:[38]

$$L = \sqrt{(a^2/3) + \{(1/2) - u\}^2 \times c^2} \quad (3)$$

where u for the wurtzite structure is given by

$$u = (a^2/3c^2) + 0.25 \quad (4)$$

and u is related to a/c. The bond lengths, L, of the ZnO lattice were 0.19648, 0.19664, 0.19668, 0.19669, and 0.19670 nm in the ZnO nanorods doped with 0, 0.5, 1.0, 2.0, and 2.5 at. % B, respectively, as shown in Fig. 2(d).

Figure 3(a) shows the normalized PL spectra for the ZnO nanorods doped with 0 - 2.5 at. % B. All the spectra show near-band-edge (NBE) emission at 3.312, 3.304, 3.302, 3.306, and 3.298 eV in the UV region for the ZnO nanorods doped with 0, 0.5, 1.0, 2.0, and 2.5 at. % B, repectively, which was generated by the recombination of free excitions.[39] In addition, all the spectra show broad deep-level emission (DLE) at 2.250, 2.251, 2.253, 2.255, and 2.251 eV in the visible region for the ZnO nanorods doped with 0. 0.5, 1.0,

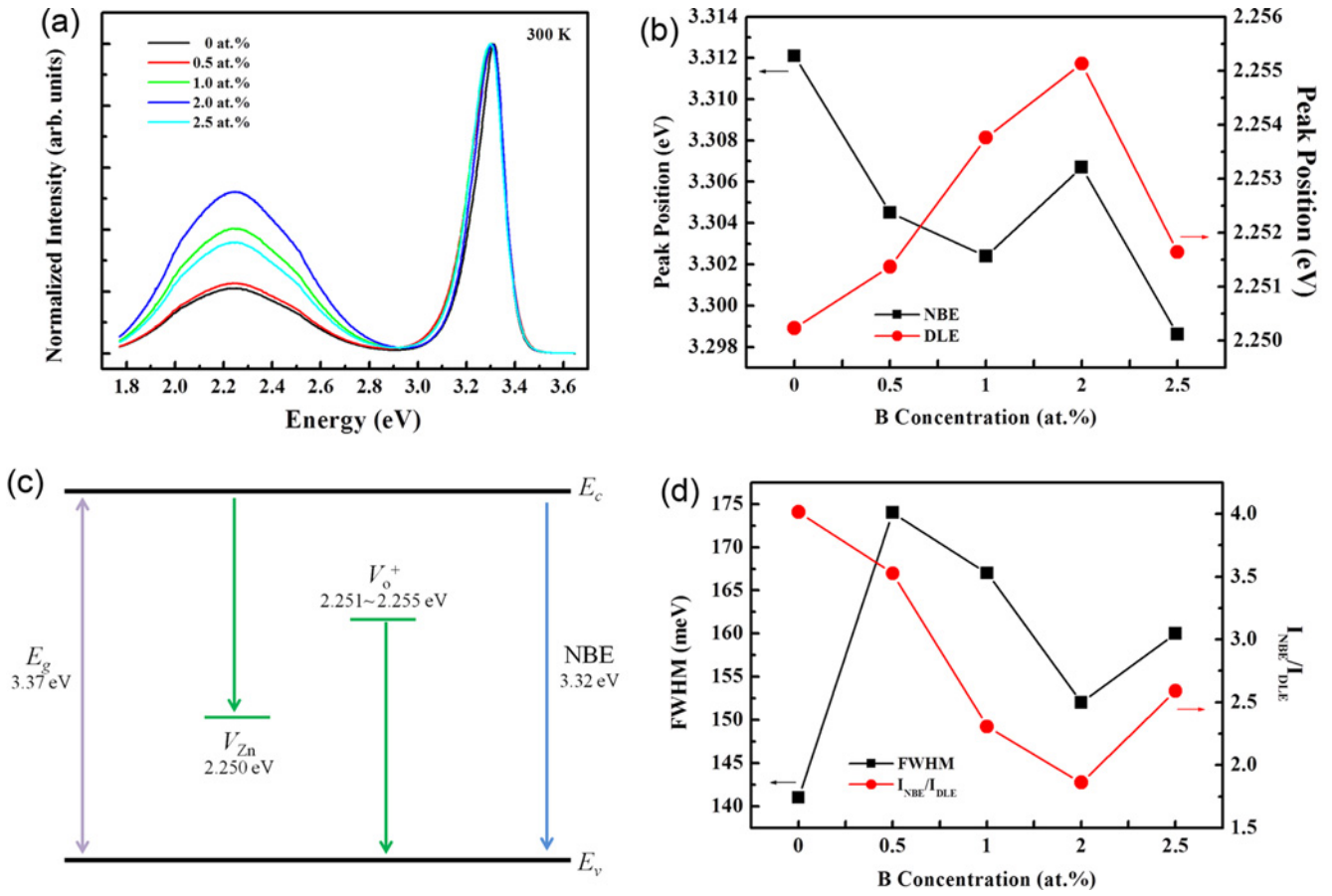

Fig. 3. (a) Normalized PL spectra, (b) positions of peaks corresponding to NBE and DLE, (c) schematic illustration of the BZO band diagram for the NBE and DLE processes, (d) FWHM and PL intensity ratio (I_{NBE}/I_{DLE}) for ZnO nanorods doped with 0 - 2.5 at. % B.

2.0, 2.5 at. % B, respectively, which is usually attributed to structural defects such as Zn vacancy (V_{Zn})[40] and singly ionized oxygen vacancy (V_O^+)[41] in the ZnO crystal lattice, which in turn produce green emission. The positions of the NBE peaks in the UV region of the spectra for the BZO nanorods shifted toward lower energies (*i.e.*, the NBE peaks were more red-shifted) than the position of the NBE peak in the UV region of the spectrum for the ZnO nanorods, as shown in Fig. 3(b). The origin of the red-shift in the NBE peaks is the residual stress (*i.e.*, tensile stress) along the *c*-axis of the ZnO crystal lattice because B doping distorted the ZnO lattice. The positions of the DLE peaks in the visible region of the spectra for the BZO nanorods, on the other hand, shifted toward higher energies (*i.e.*, the DLE peaks were more blue-shifted) than the position of the DLE peak in the visible region of the spectrum for the ZnO nanorods. The blue-shift in the DLE peaks indicates the variation in the relative contributions of various possible B-doping-induced defects in the ZnO crystal lattice. V_{Zn} and V_O^+ are the most probable defects in the ZnO crystal lattice of the BZO nanorods and are responsible for green emission and the blue-shift in the DLE peaks in the spectra for the BZO nanorods as shown in Fig. 3(c). Figure 3(d) shows the full width at half maximum (FWHM) and the ratios of the NBE to DLE (I_{NBE}/I_{DLE}) PL intensities (*i.e.*, the PL intensity ratios) for the ZnO nanorods doped with 0 - 2.5 at. % B. The FWHMs were 141, 174, 167, 152, and 160 meV for the ZnO nanorods doped with 0, 0.5, 1.0, 2.0, 2.5 at. % B, repectively. Although the FWHM for the ZnO nanorods doped with 2.0 at. % B was the narrowest among the FWHMs for all the BZO nanorods, it was still wider than that for the undoped ZnO nanorods. The PL intensity ratio were 4.014, 3.526, 2.306, 1.816, and 2.590 for the ZnO nanorods doped with 0, 0.5, 1.0, 2.0, 2.5 at. % B, respectively. The PL ratios gradually decreased with increasing concentration of B in the nanorods to 2.0 at. % and then increased again for the ZnO nanorods doped with 2.5 at. % B. Hence, doping the ZnO nanorods with B significantly varied the PL properties of the ZnO nanorods, so it is possible to tune the DLE of the ZnO nanorods as the need arises in various applications such as chemical gas sensors, solar cells, lighting emitting diodes, etc.

Figure 4 shows the electrical properties (*i.e.*, resistivity ρ, carrier concentration N_e, and hall mobility μ) of the nanorods

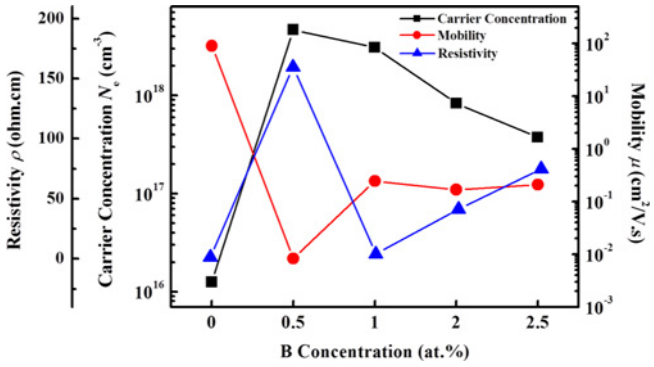

Fig. 4. Dependence of electrical properties (*i.e.*, resistivity ρ, carrier concentration N_e, and hall mobility μ) of nanorods plotted as function of B concentration for ZnO nanorods doped with 0 - 2.5 at. % B.

plotted as functions of the concentration of B in the nanorods. The values of N_e for all the BZO nanorods were significantly higher than that for the undoped ZnO nanorods. The values of N_e were 1.252×10^{16}, 4.662×10^{18}, 3.079×10^{18}, 8.289×10^{17}, and 3.741×10^{17} cm^{-3} for the ZnO nanorods doped with 0, 0.5, 1.0, 2.0, and 2.5 at. % B, respectively. Doping the nanorods with B also varied the ρ and μ of the nanorods. The ρ and μ were 5.530, 161.7, 8.219, 44.8, and 78.1 Ω·cm and 9.007×10^{1}, 8.275×10^{-3}, 2.466×10^{-1}, 1.677×10^{-1}, and 2.136×10^{-1} cm^2/V·s for the ZnO nanorods doped with 0, 0.5, 1.0, 2.0, and 2.5 at. % B, respectively. The ρ of the BZO nanorods were higher than that of the undoped ZnO nanorods, which can be explained by the limit of the solubility of B in the ZnO lattice.[42] The μ of the BZO nanorods were lower than that of the undoped ZnO nanorods, which can be explained by ionized impurity scattering[43] and may indicate that the ZnO lattice had been doped with interstitial B^{3+} ions and/or that the Zn^{2+} ions in the ZnO crystal lattice had been substituted with the higher valence B^{3+} ions. Furthermore, the formation of an electron killer (*i.e.*, V_{Zn}), which has been theoretically observed,[44] could decrease the concentration of carriers with increasing concentration of B in the nanorods. Thus, the increase again in the ρ of the ZnO nanorods doped with above 1.0 at. % B might be because the higher concentration of B increased the number of sites at which ionized impurity and grain boundary scattering occur in the BZO nanorods, leading to lower μ for lower N_e for concentrations of B above 1.0 at. %.

4. CONCLUSIONS

ZnO seed layers were deposited onto quartz substrates using the sol-gel spin-coating, and ZnO nanorods doped with 0 - 2.5 at. % B were hydrothermally grown on the ZnO seed layers. All the nanorods grown in this experiment were uniform and hexagonal. Furthermore, doping the nanorods with B significantly varied the structural, optical, and electrical properties of ZnO nanorods, such as the length of nanorods, lattice constants, residual stress, bond length, PL, ρ, N_e, and μ. B-doping-induced change in the lattice structure and/or crystallinity of the ZnO nanorods is desirable because the ZnO lattice constants are close to the reported values and strain-free ZnO with increasing concentrations of B in the nanorods. From the PL and Hall-effect data, it is possible to tune the DLEs, ρ, N_e, and μ of BZO nanorods as the need arises in various applications such as transparent conducting oxide, chemical gas sensors, solar cells, light-emitting diodes, etc.

ACKNOWLEDGMENTS

This research was supported by Basic Science Research Program through the National Research Foundation of Korea (NRF) funded by the Ministry of Education, Science and Technology (No. 2012R1A1B3001837).

REFERENCES

1. M. Willander, O. Nur, Q. X. Zhao, L. L. Yang, M. Lorenz, B. Q. Cao, J. Z. Pérez, C. Czekalla, G. Zimmermann, M. Grundmann, A. Bakin, A. Behrends, M. A. Suleiman, A. E. Shaer, A. C. Mofor, B. Postels, A. Waag, N. Boukos, A. Trvalos, H. S. Kwack, J. Guinard, and D. L. S. Dang, *Nanotechnology* **20**, 332001 (2009).
2. S. Kim, M. S. Kim, K. G. Yim, G. Nam, D.-Y. Lee, J. S. Kim, J. S. Kim, J.-S. Son, and J.-Y. Leem, *J. Korean Phys. Soc.* **60**, 1599 (2012).
3. R. C. Pawar, J. S. Shaikh, S. S. Suryavanshi, and P. S. Patil, *Curr. Appl. Phys.* **12**, 778 (2012).
4. R. C. Pawar, H.-S. Kim, and C. S. Lee, *Scripta Mater.* **68**, 142 (2013).
5. R. C. Pawar, J.-W. Lee, V. B. Patil, and C. S. Lee, *Sensor. Actuat. B: Chem.* (in press).
6. A. Tubtimtae and M.-W. Lee, *Superlattices. Microstruct.* **52**, 987 (2012).
7. H. Yang, J.-S. Lee, S. Bae, and J. H. Hwang, *Curr. Appl. Phys.* **9**, 797 (2009).
8. T.-H. Fang and S.-H. Kang, *J. Phys. D: Appl. Phys.* **41**, 245303 (2008).
9. F. S.-S. Chien, C.-R. Wang, Y.-L. Chan, and H.-L. Lin, *Sens. Actuators, B* **144**, 120 (2010).
10. S. Oh, M. Jung, J. Koo, Y. Cho, S. Choi, S. Yi, G. Kil, and J. Chang, *Physica E,* **42**, 2285 (2010).
11. S. Kim, G. Nam, H. Park, H. Yoon, S.-H. Lee, J. S. Kim, J. S. Kim, D. Y. Kim, S.-O. Kim, and J.-Y. Leem, *Bull. Korean Chem. Soc.* **34**, 1205 (2013).
12. D. Y. Kim, S.-O. Kim, M. S. Kim, K. G. Yim, S. Kim, G. Nam, D.-Y. Lee, and J.-Y. Leem, *J. Korean Phys. Soc.* **60**, 9498 (2012).
13. Z. Tian, J. A. Voigt, J. Liu, B. Mckenzie, M. J. Mcdermott, M. A. Rodriguez, H. Konishi, and H. Xu, *Nat. Mater.* **2**, 821 (2003).

14. Q. Yu, L. Li, H. Li, S. Gao, D. Sang, J. Yuan, and P. Zhu, *Appl. Surf. Sci.* **257**, 5984 (2011).
15. V. Kumar, R. G. Singh, L. P. Purohit, and R. M. Mehra, *J. Mater. Sci. Technol.* **27**, 481 (2011).
16. S. Kim, M. S. Kim, G. Nam, and J.-Y. Leem, *Electron. Mater. Lett.* **8**, 445 (2012).
17. B. G. Choi, I. H. Kim, D. H. Kim, K. S. Lee, T. S. Lee, B. Cheong, Y.-J. Baik, and W. M. Kim, *J. Eur. Ceram. Soc.* **25**, 2161 (2005).
18. L. Zhu, J. Li, Z. Ye, H. He, X. Chen, and B. Zhao, *Opt. Mater.* **31**, 237 (2008).
19. G. Pineda-Hernandez, A. Escobedo-Morales, U. Pal, and E. Chigo-Anota, *Mater. Chem. Phys.* **135**, 810 (2012).
20. A. E. Morales, M. H. Zaldivar, and U. Pal, *Opt. Mater.* **29**, 100 (2006).
21. T.-H. Fang and S.-H. Kang, *Curr. Appl. Phys.* **10**, 1076 (2010).
22. J. Jie, G. Wang, X. Han, and J. G. Hou, *J. Phys. Chem. B* **108**, 17027 (2004).
23. L. Xu, Y. Su. Y. Chen, H. Xia, L. Zhu, Q. Zhou, and S. Li, *J. Phys. Chem. B* **110**, 6637 (2006).
24. M. Snure and A. Tiwari, *J. Appl. Phys.* **104**, 073707 (2008).
25. X. G. Xu, H. L. Yang, Y. Wu, D. L. Zhang, S. Z. Wu, J. Miao, Y. Jiang, X. B. Qin, X. Z. Cao, and B. Y. Wang, *Appl. Phys. Lett.* **97**, 232502 (2010).
26. B. N. Pawar, G. Cai, D. Ham, R. S. Mane, T. Ganesh, A. Ghule, R. Sharma, K. D. Jadhava, and S.-H. Han, *Sol. Energ. Mat. Sol. C.* **93**, 524 (2009).
27. J. Steinhauser, S. Fay, N. Oliveria, E. Vallat-Sauvain, and C. Ballif, *Appl. Phys. Lett.* **90**, 142107 (2007).
28. S. Colis, H. Bieber, S. B-Colin, G. Schmerber, C. Leuvrey, and A. Dinia, *Chem. Phys. Lett.* **422**, 529 (2006).
29. S. Deka and P. A. Joy, *Solid State Commun.* **142**, 190 (2007).
30. J.-S. Hur, J. Kim, S. Jang, J.-B. Song, D. Byun, C.-S. Son, J. H. Yun, and K. H. Yoon, *J. Korean Phys. Soc.* **53**, 442 (2008).
31. Q. Yu, J. Li, H. Li, Q. Wang, S. Cheng, and L. Li, *Chem. Phys. Lett.* **539**, 74 (2012).
32. B. Gupta, A. Jain, and R. M. Mehra, *J. Mater. Sci. Technol.* **26**, 223 (2010).
33. S. Fujihara, A. Suzuki, and T. Kimura, *J. Appl. Phys.* **94**, 2411 (2003).
34. W.-J. Li, E.-W. Shi, W.-Z. Zhong, and Z.-W. Yin, *J. Cryst. Growth* **203**, 186 (1999).
35. R.B. Heller, J. McGannon, and A. H. Weber, *J. Appl. Phys.* **21**, 1283 (1950).
36. G. Nam, S. Kim, M. S. Kim, K. G. Yim, D. Y. Kim, S.-O. Kim, and J.-Y. Leem, *J. Korean Phys. Soc.* **59**, 129 (2011).
37. J.-W. Jeon, M. Kim, L.-W. Jang, J. L. Hoffman, N. S. Kim, and I.-H. Lee, *Electron. Mater. Lett.* **8**, 27 (2012).
38. M. S. Kim, K. G. Yim, S. Kim, G. Nam, D.-Y. Lee, J. S. Kim, J. S. Kim, and J.-Y. Leem, *J. Korean Phys. Soc.* **59**, 2354 (2011).
39. S. Kim, G. Nam, K. G. Yim, J. Lee, Y. Kim, and J.-Y. Leem, *Electron. Mater. Lett*. **9**, 293 (2013).
40. F. Tuomisto, K. Saarinen, D. C. Look, and G. C. Farlow, *Phys. Rev. B* **72**, 085206 (2005).
41. A. B. Djurisic, Y. H. Leung, K. H. Tam, L. Ding, W. K. Ge, H. Y. Chen, and S. Gwo, *Appl. Phys. Lett.* **88**, 103107 (2006).
42. B. N. Pawar, S. R. Jadkar, and M. G. Takwale, *J. Phys. Chem. Solids* **66**, 1779 (2005).
43. F. Ruske, M. Roczen, K. Lee, M. Wimmer, S. Gall, J. Hupkes, D. Hrunski, and B. Rech, *J. Appl. Phys.* **107**, 013708 (2010).
44. S. Lany and A. Zunger, *Phys. Rev. Lett.* **98**, 045501 (2007).